Investigating the Control by Quantum Confinement and Surface Ligand Coating of Photocatalytic Efficiency in Chalcopyrite Copper Indium Diselenide Nanocrystals

Atanu Jana,[1,#,$] Katie N. Lawrence,[1,#] Meghan B. Teunis,[1] Manik Mandal,[2] Amar Kumbhar,[3] and Rajesh Sardar[1,4,]*

[1]Department of Chemistry and Chemical Biology, Indiana University-Purdue University Indianapolis, 402 N. Blackford Street, Indianapolis, Indiana 46202, United States

[2]Department of Chemistry, Lehigh University, 6 East Packer Avenue, Bethlehem, Pensylvania18015, United States

[3]Chapel Hill Analytical and Nanofabrication Laboratory, University of North Carolina, Chapel Hill, North Carolina, 27599, United States

[4]Integrated Nanosystems Development Institute, Indiana University-Purdue University Indianapolis, 402 N. Blackford Street, Indianapolis, Indiana 46202, United States

[$]Present address: Department of Chemistry, Indian Institute of Technology, Hauz Khas, New Delhi, 110016, India

---

This is the author's manuscript of the article published in final edited form as:
Jana, A., Lawrence, K. N., Teunis, M. B., Mandal, M., Kumbhar, A., & Sardar, R. (2016). Investigating the Control by Quantum Confinement and Surface Ligand Coating of Photocatalytic Efficiency in Chalcopyrite Copper Indium Diselenide Nanocrystals. Chemistry of Materials, 28(4), 1107–1120. http://doi.org/10.1021/acs.chemmater.5b04521

ABSTRACT: In the past few years, there has been an immense interest in the preparation of sustainable photocatalysts composed of semiconductor nanocrystals (NCs) as one of their component. We report here, for the first time, the effects of structural parameters of copper indium diselenide ($CuInSe_2$) NCs on visible light driven photocatalytic degradation of pollutants under homogeneous conditions. Ligand exchange reactions were performed replacing insulating, oleylamine capping with poly(ethylene glycol) thiols to prepare PEG-thiolate-capped, 1.8 to 5.3 nm diameter $CuInSe_2$ NCs to enhance their solubility in water. This unique solubility property caused inner-sphere electron transfer reactions (O_2 to O_2•−) to occur at the NCs surface allowing for sustainable photocatalytic reactions. Electrochemical characterization of our dissolved $CuInSe_2$ NCs showed that the thermodynamic driving force (-ΔG) for oxygen reduction, which increased with decreased NCs size, was the dominant contributor to the overall process when compared to the contribution light absorption and the coulombic interaction energies of electron-hole pair ($J_{e/h}$). A two-fold increase in phenol degradation efficiency (from 30 to ~60%) was achieved by controlled variation of the diameter of $CuInSe_2$ NCs from 5.3 to 1.8 nm. The surface ligand dependency of photocatalytic efficiency was also investigated and a profound effect on phenol degradation was observed. Our PEG-thiolate-capped $CuInSe_2$ NCs showed photocatalytic activity towards other organic compounds, such as N, N-dimethyl-4-phenylenediamine, methylene blue, and thiourea, which showed decomposition under visible light.

INTRODUCTION

Simple and cost effective destruction of toxic organic pollutants is an ever-increasing need. Sunlight is the most abundant energy source, which can be used to perform various photocatalytic reactions mediated by semiconductor nanocrystals (NCs).[1-6] Given the NC composition, there are two important structural parameters - size ("quantum confinement effect") and the surface ligand chemistry of NCs - that control light absorption, enhance photogenerated charge separation, and reduce charge recombination, which together determine the catalytic efficiency.[7-14] Anatase TiO_2 is considered to be the most efficient and environmentally friendly photocatalyst.[15] However, its large band gap (~3.4 eV) allows only ultraviolet light absorption, which hinders its potential photocatalytic applications and commercialization. The size dependency of photocatalytic solar hydrogen production[16, 17] and water splitting[2, 18] were investigated using suspended CdE (E = S and Se) quantum dots (QDs) as a model system, but Cd cytotoxicity hinders their use in future applications. In addition, quantitative information about (1) energy levels of the highest occupied (HOMO) and lowest unoccupied (LUMO) molecular orbitals and (2) coulombic interaction energy of photogenerated electron hole-pair ($J_{e/h}$) in NCs are extremely important to facilitate interfacial (e.g., solid-liquid) charge transfer to prepare unique nanomaterials with advanced photocatalytic activities. In this article we report for the first time a correlation between size and thermodynamic driving force ($-\Delta G$) for molecular oxygen reduction, which controlled the photocatalytic efficiency of chalcopyrite copper indium diselenide ($CuInSe_2$) NCs under homogeneous reaction condition.

In recent years, copper-based ternary semiconductor NCs (e.g., $CuInS_2$ and $CuInSe_2$) have shown immense promise as sensitizers in designing solar cells aimed at replacing environmentally toxic elements (e.g., Cd and Pb).[19-23] Moreover, these NCs display band-gaps of

<1.5 eV, which are in the visible region of the solar spectrum, and large absorption coefficients that are ideal for solar energy conversion.[24-26] In this context, there are few reports available demonstrating the photocatalytic activity of these NCs, and in all cases they were used in sensitizing wide band-gap semiconductors (e.g., ZnS, ZnO, and TiO_2).[19, 27, 28] To the best of our knowledge, no experimental reports are available showing quantum-confinement controlled photocatalytic degradation of pollutants [e.g., phenol, dimethyl-4-phenylenediamine (DMPD), methylene blue, and thiourea] in water with $CuInSe_2$ NCs, as presented in this article.

To better understand the effect of size and surface ligand chemistry of $CuInSe_2$ NCs on photocatalytic efficiency, we first develop a non-phosphinated synthetic method to prepare oleylamine (OLA)-coated, 1.8 to 5.3 nm NCs. Ligand exchange reactions were performed with polyethylene glycol (PEG)-thiols with varying glycol units (n = 6, 18, 60, 150) to replace the insulating ligand OLA in order to enhance the solubility properties in water and to facilitate *inner-sphere* electron transfer reaction. For the first time, we investigated size-dependent electrochemical properties of fully diffused $CuInSe_2$ NCs, through cyclic voltammetry (CV) and have shown the most pristine voltammograms ever reported for semiconductor NCs. A combined electrochemical and optical characterization demonstrated that the smallest diameter NCs exhibited the most efficient interfacial electron transfer and reached a $-\Delta G$ up to 0.254 eV for reduction of O_2 to $O_2^{\bullet -}$. This facile electron transfer enhanced phenol degradation efficiency up to ~60% for 1.8 nm diameter NCs. We have also shown that a nearly four-fold higher catalytic efficiency could be achieved for PEG_6-thiolate-coated $CuInSe_2$ NCs *versus* those coated with OLA or PEG_{150}-thiolate. We believe, our experimental results will facilitate the use of ternary semiconductor NCs as photocatalysts for solar energy conversion. Moreover, the unique solubility properties of the PEG-thiolate-coated $CuInSe_2$ NCs will allow the detailed study of charge transfer dynamics[7, 8] to enhance our fundamental understanding of electronic properties for faster and highly efficient catalytic reactions.

RESULTS AND DISCUSSION

Synthesis and Characterization of Oleylamine-Coated $CuInSe_2$ NCs. In order to determine the quantum confinement effects on photocatalytic efficiency of $CuInSe_2$ NCs, we developed a new phosphine-free synthetic method to prepare ~1.0 to 5.3 nm NCs. As detailed more fully in the Methods section, CuCl and $InCl_3$ were mixed with OLA in a 25 ml two-neck round-bottom flask at 130 °C. The reaction mixture was stirred under vacuum for 2 h and then switched to N_2 and stirred for another 1 h. Separately, Se-precursor was prepared by dissolving Se powder in a mixture OLA and hexanethiol at room temperature. The precursor was stirred for 90 min at room temperature under N_2 atmosphere. Next, Se-precursor was injected into the metal precursor and the formation of $CuInSe_2$ NCs was monitored by UV-visible spectroscopy at different time points, as shown in Figure 1A. The continuous red-shifting of the absorption peak – 697, 735, and 777 nm at 15, 30, and 60 min, respectively – suggests an increase in NC's size over time due to the growth process. The detailed growth mechanism for the formation of $CuInSe_2$ NCs was reported earlier and believed to be the initial formation of binary metal selenides, which fused together yield $CuInSe_2$ NCs.[29]Approximately 90 min after the injection of the Se-precursor, a stable absorption peak at ~800 nm was observed and no further shift in the peak position was observed upon heating for an additional 30 min, indicating the growth was completed at the 90 min time point. The $CuInSe_2$ NCs were purified using the solvent arrested precipitation technique and the detail procedure is presented in the Materials and Methods section. Different sizes of $CuInSe_2$ NCs were synthesized by a systematic manipulation of the reaction parameters such as reaction temperature, growth time, and amount of Se-precursor, as listed in Table 1.

Figure 1B illustrates the UV-visible absorption spectra of different sizes of $CuInSe_2$ NCs where the temperature of the precursors at the injection time was varied from 100 – 150 °C. It appears that the absorption peak red-shifted due to the increase in size as a consequence of quantum confinement, as reported in the literature.[30, 31] We determined the optical band-gap (in eV) directly from the band-edge absorption peak.

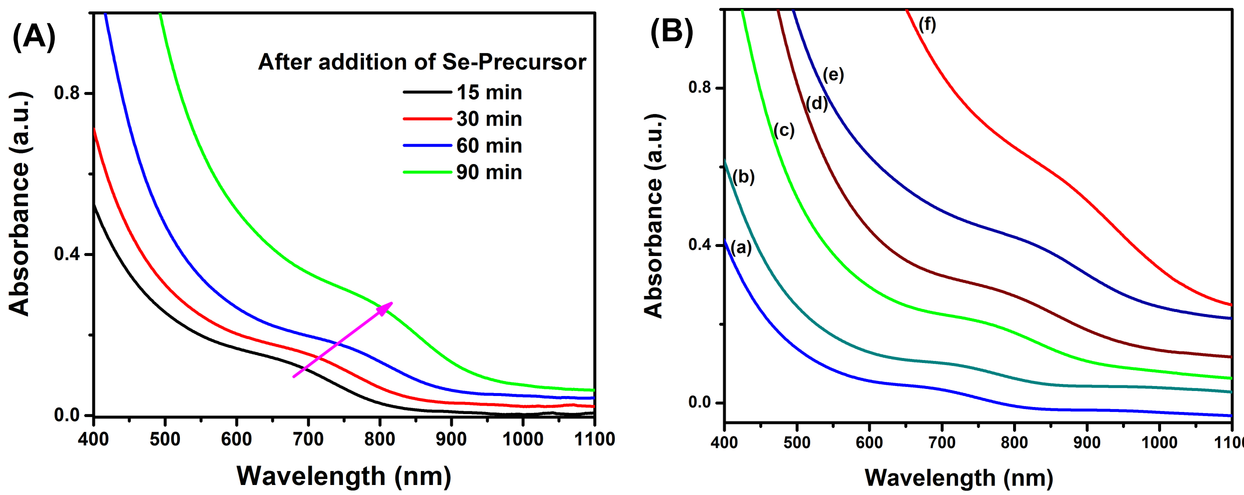

Figure 1. (A) UV-visible absorption spectra of $CuInSe_2$ NCs at different time points of the synthesis after addition of Se-precursor at 130 °C. (B) UV-visible absorption spectra of $CuInSe_2$ NCs synthesized at (a) 100, (b) 110, (c) 120, (d) 130, (e) 140, and (f) 150 °C. Each sample was purified by solvent arrested precipitation before optical analysis. All spectra were collected in toluene.

TABLE 1. Comparison of UV-visible Absorption Peak Position, Optical Band-Gap, and Size of $CuInSe_2$ NCs at Different Time Intervals After Injection of Se-Precursor

growth temperature (°C)	time (min)	absorption peak position (nm)	optical band-gap (eV)	NCs size (nm)[b,c,d]
100	150	705	1.76	-
110	90	740	1.67	1.8 (0.4)
120	90	765	1.62	2.4 (0.5)
130	90	800	1.55	3.5 (0.8)
140	120	845	1.47	4.1 (0.9)

150	180	915[a]	1.35	5.3 (1.2)

[a]The synthesis was conducted using (0.825 mL, 0.627 mmol) of Se-precursor and all other reaction conditions were identical. [b]In each case, 300 NCs were counted to determine the size and the size dispersion. [c]The $CuInSe_2$ NCs were close to 1.0 nm, and we were unable to determine the diameter due to very low contrast in the TEM image. [d]The number in the parentheses indicates the standard deviation.

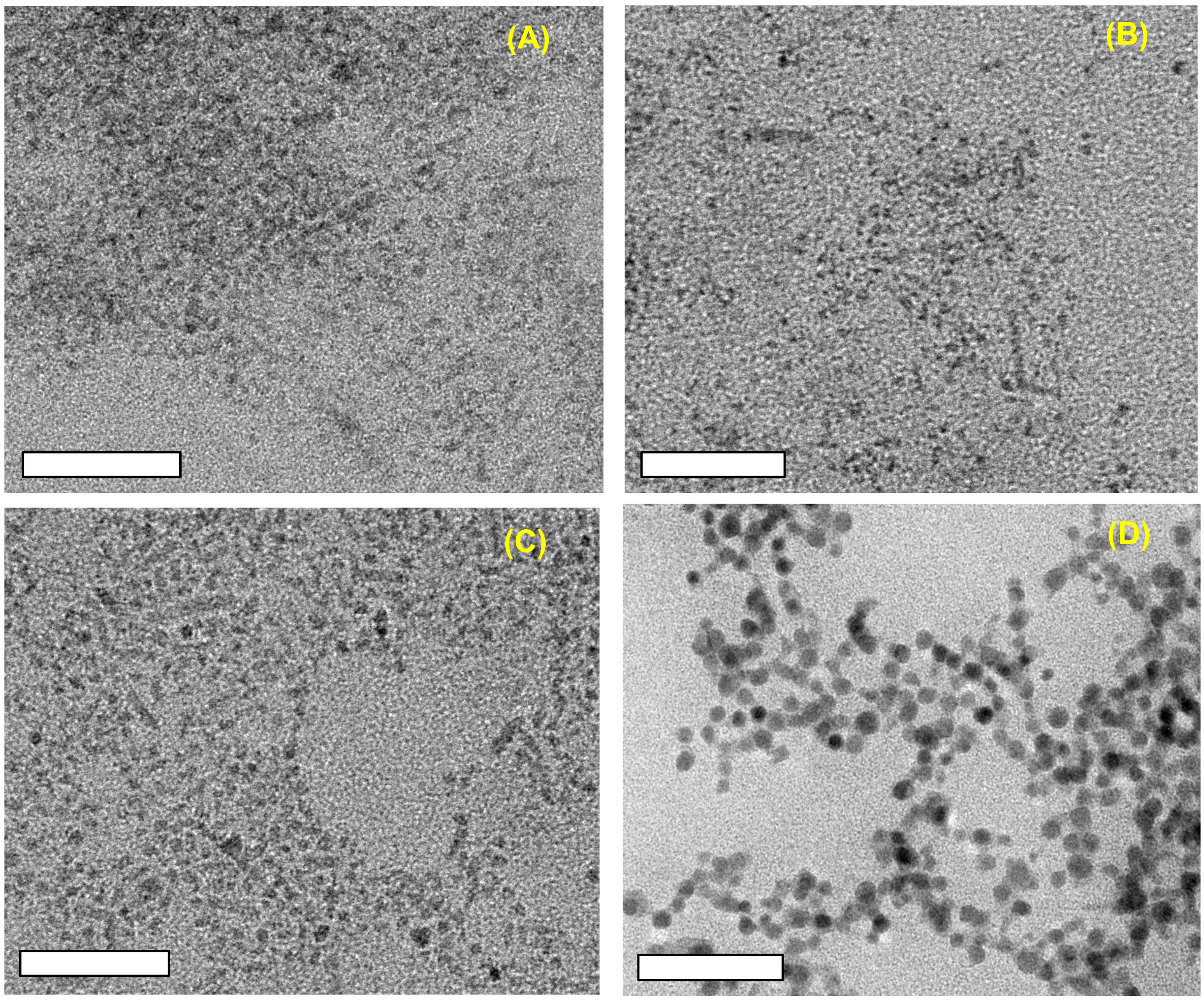

Figure 2. TEM images of $CuInSe_2$ NCs displaying different UV-visible absorption peak positions: (A) 705, (B) 740, (C) 800, and (D) 915 nm. The corresponding average diameter is listed in Table 1. Scale bars are 100 nm.

The size of the $CuInSe_2$ NCs was determined by transmission electron microscopy (TEM) of the purified samples. Figure 2 shows the TEM images of the $CuInSe_2$ NCs. The average size of the NCs synthesized using our phosphine-free approach is listed in Table 1 and Figure S1. High-resolution TEM analysis showed that all the NCs appeared to be spherical in shape (Figure S2). It is evident the size of the NCs can be controlled by manipulating the reaction temperature, growth time, and amount of Se-precursor used in the synthesis. We performed an X-ray diffraction (XRD) analysis to determine the structural phases of our $CuInSe_2$ NCs. Figure 3A illustrates the XRD pattern of the $CuInSe_2$ NCs, which were synthesized at different temperatures. The XRD pattern of the NCs did match the diffraction pattern as reported earlier for $CuInSe_2$ NCs[21, 32] and JCPDS database (JCPDS no. 75-0107). Importantly, the appearance of a diffraction peak of (211) at 35.68° (Figure S3) of $CuInSe_2$ NCs suggests the chalcopyrite phase as opposed to the sphalerite phase.[33] As expected, the diffraction peaks became shaper as the size increased, which is due to better crystallinity character. We also analyzed the chemical composition of $CuInSe_2$ NCs by energy dispersive X-ray (EDS) analysis and a representative EDS spectrum is shown in Figure 3B. Analysis of five randomly selected areas provided an average Cu:In:Se composition of 0.94:0.79:2.00. The $CuInSe_2$ NCs were slightly Cu- (Cu/In = 1.19) and Se- [Se/(Cu +In) = 1.16] rich. The formation of Se-rich NCs is also supported by a broad photoluminescence (PL) peak and very low peak intensity (see Figure S4). Similar PL characteristics were previously reported for Se-rich CdSe quantum dots.[34] The surface of our $CuInSe_2$ NCs is coated with OLA, which is a L-type ligand[35-37] and only passivates surface metal sites, leaving the Se sites unpassivated. This type of surface chemistry creates dangling bonds and defect sites that together reduce the PL properties. Cu- and Se-rich $CuInSe_2$ NCs and unpassivated surface Se-sites decrease the PL properties. Perhaps, post-synthetic surface ligand treatment[38, 39] of OLA-coated $CuInSe_2$ NCs could partially enhance the PL emission characteristic by passivating nonradiative trap states, which is currently under investigation.

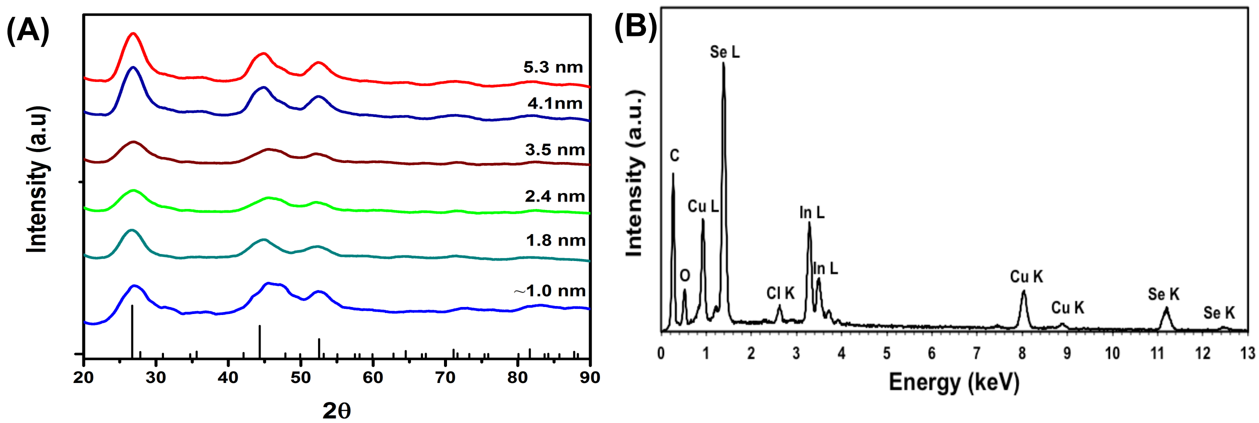

Figure 3. (A) XRD patterns of different sized $CuInSe_2$ NCs. The stick pattern represents bulk tetragonal chalcopyrite $CuInSe_2$ (JCPDS#75-0107) is shown as a reference. (B) A representative EDS spectrum of purified $CuInSe_2$ NCs.

Our synthetic approach for the preparation of different sizes of $CuInSe_2$ NCs is markedly different than literature procedures. Firstly, we synthesized our NCs at moderately low temperature (100 -150 °C) in comparison to other non-phosphinated methods, which required very high temperature (240 -290 °C).[23, 33, 40-43]Secondly, the NCs described in the literature are either polydispersed and much larger in diameter (~30 nm),[44] or anisotropic in shape[45, 46] in comparison to our spherically-shaped <6.0 nm diameter $CuInSe_2$ NCs. Lastly and most importantly, our phosphine-free synthetic procedure is nontoxic compared to other methods, which use unstable and hazardous, trioctylphosphine, tributylphosphine, and diphenylphosphine to dissolve elemental Se.[21, 32, 47-49] We believe our size-controlled synthesis of $CuInSe_2$ NCs at

<150 °C could be due to the high reactivity of the Se-precursor $[(Se)_m(OLA)_n]$ used in the synthesis.[50] We and others have previously used a similar Se-precursor for the synthesis of CdSe QDs,[38] Cu_2SnSe_3,[51] and $Cu_2ZnSnSe_4$ NCs,[50] respectively. Here have demonstrated the first, non-phosphinated synthetic route to prepare nearly monodispersed $CuInSe_2$ NCs (<6.0 nm in diameter) coated with soft-ligand OLA at moderately low temperature.[52] The purified NCs were found to be stable for at least a week inside a N_2-filled glovebox. The soft ligand coating provided us the unique opportunity to modify the surface of the NCs with ligands, which not only enhance the solubility properties but also facilitate charge transfer process for sustainable photocatalytic applications, as discussed later.

Size Dependent Electrochemical Properties of Fully Diffused $CuInSe_2$ NCs in Solution. Because of the increasing potential for application in solar cells and photocatalysis, it is important to determine the energy level position of HOMO and LUMO, $J_{e/h}$ of semiconductor NCs, flat-band potential to extract the maximum number of charge carriers. This critical information cannot be determined by simple optical absorption measurements. Since the initial report of determining size-dependent electrochemical band-gap of dispersed CdS NCs in DMF/electrolyte, electrochemical properties of dispersed CdSe,[53-60] CdTe,[53, 61, 62] CdS_xSe_{1-x},[63] and $CdSe_xTe_{1-x}$,[64] NCs were also investigated, but to the best of our knowledge size-dependent electrochemical characterization of $CuInSe_2$ NCs has not been reported. However, in all cases appearance of multiple peaks in the CV were observed, which could be either presence of free, unbound surface passivating ligands and/or existence of surface trap states of NCs.[53, 58] Additionally electrochemical measurements are frequently conducted in a solvent system (toluene) that does not allow for a large window potential scan.[65] Moreover, it has also been reported that optical band-gap $\left(E_{gap}^{opt}\right)$ is higher than the electrochemical band-gap $\left(E_{gap}^{el}\right)$ and according to Eq. 1.[31, 53, 66] this confounds the quantum confinements. We suggest that the NCs were not completely soluble in the solvent/electrolyte media, and thus electron injection and extraction processes may have been hindered by slow charge transfer kinetics.

$$E_{gap}^{el} = E_{gap}^{opt} + J_{e/h} \qquad (1)$$

Recently, size- and composition-dependent electrochemistry of copper-based ternary semiconductor (e.g., $CuInS_2$, Cu_2SnSe_3, and CuZnSeS) NCs were investigated using CV technique where NCs were deposited as a film onto an electrode surface.[67-69] However, such current potential profiles do not represent the electrochemical characteristics (position of the HOMO and LUMO, and also E_{gap}^{el}) of fully diffused and isolated NCs. This is because the NCs are present in an aggregated state in the film, which results in discrepancy in the quantum confinement effects, as reported for Cu_2SnSe_3 NCs.[69] Moreover, an insulating ligand coating [OLA and/or dodecanethiol (DDT)] inside the NCs film would cause a sluggish electron transfer which could trigger chemical reactions inside the film, causing a change in the film morphology and degradation of the sample. Therefore, current literature reports[67-70] demonstrating electrochemical information of copper-based ternary semiconductor NCs may not represent quantitative information about the HOMO and/or LUMO position and $J_{e/h}$. To overcome the above-mentioned limitations in electrochemical analysis and to fully exploit the potential application of semiconductor NCs as photocatalysts, we here report for the first time the design of a unique ligand-coated semiconductor NC system that is completely soluble in an electrochemically friendly solvent (e.g., acetonitrile) to perform solution electrochemistry of fully diffused NCs.

In our initial investigation, electrochemistry of OLA-coated, different-sizes of $CuInSe_2$ NCs dispersed in a toluene/DCM/Bu_4NPF_6 solution showed an appearance of multiple peaks in CV (Figure S5). In the voltammograms we used onset potentials from which oxidation (removal of electrons from HOMO) and reduction (addition of electrons to LUMO) waves appeared to calculate E_{gap}^{el} and $J_{e/h}$ values. To perform a solution-phase electrochemical analysis of OLA-coated $CuInSe_2$ NCs, 0.02 mmol of the NCs were suspended in a 3.0 mL (1:5 mixture of toluene:DCM) 0.1 M Bu_4NPF_6 electrolyte solution. Figure S4 shows the CV of different-sizes $CuInSe_2$ NCs in which onset of oxidation and reduction peaks were used to determine the E_{gap}^{el}. Importantly, the E_{gap}^{el} is higher than the E_{gap}^{opt} (see Table S1), which is in agreement with the theoretical calculation.[53] Higher E_{gap}^{el} and $J_{e/h}$ for smaller NCs nicely corroborated with size-dependent quantum confinement as well.[31]

However, some unwanted features appeared in the voltammograms. Firstly, several peaks were observed (Figure S4, black dots), which do not correspond to the HOMO or LUMO states. These peaks could correspond to the presence of deep and surface trap states, as previously described in electrochemical characterization of CdSe QDs.[56, 58] Secondly, a large oxidation peak current was observed at higher potential (after the band-gap). It is know that OLA could undergo dynamic exchange and be present unbound in solution[71] and thus we believe large anodic peak current could be due to oxidation of free OLA. Thirdly, after two potential cycle scan (+1.8 to -2.5 V vs. Ag QRE) we observed the appearance of a brown precipitate at the bottom of the electrochemical cells, which was not soluble in toluene. We believe that the OLA-coated $CuInSe_2$ NCs decomposed during the potential scanning. Therefore, electrochemical data may not represent the true value of E_{gap}^{el} and $J_{e/h}$ and perhaps, insulating ligands such as OLA-coating used in our study, or trioctylphisphine-, stearic acid-, and DDT-coated semiconductor

NCs[55, 60, 62, 64, 67, 68] may not be suitable for quantitative electrochemical characterization and further determination of electronic and thermodynamic parameters.

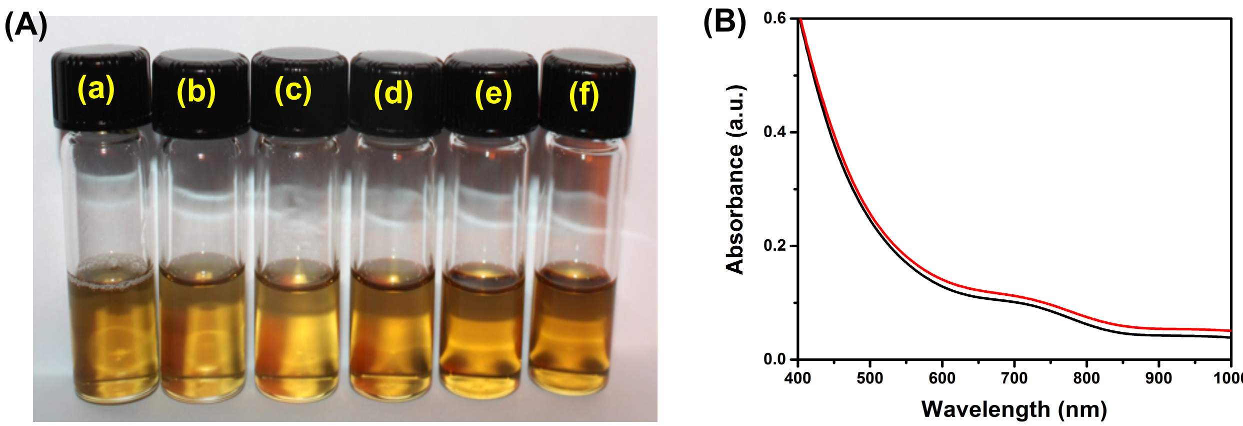

Figure 4. (A) Photograph of PEG_6-thiolate-coated $CuInSe_2$ NCs dissolved in different solvents: (a) water, (b) ethanol, (c) acetonitrile, (d) benzonitrile, (e) chloroform, and (f) dichloromethane. (B) UV-visible absorption spectra of 1.8 nm diameter $CuInSe_2$ NCs coated with OLA (black) and PEG_6-thiolate (red).

Recently, we have shown that exchanging the hydrophobic ligand, OLA from the surface of CdSe QDs with PEG_n-thiols (n = 6, 18, 60, and 150) resulted in diverse solubility properties of newly formed PEG_n-thiolate-coated QDs. These QDs are soluble in electrochemistry friendly solvent like acetonitrile and DCM.[72] Moreover, these two solvents allow electrochemical measurements in a larger potential window,[65] which is critical to precisely determine the E_{gap}^{el} and $J_{e/h}$ for smaller NCs.[59] Furthermore, polyether chains such as PEG display *"solvent-like"* properties and enable faster charge transport through the polymer layers.[73, 74] In the quest of obtaining clear voltammograms of semiconductor NCs, we decided to study the electrochemistry of dissolved PEG_6-thiolate-coated $CuInSe_2$ NCs in Bu_4NPF_6/CH_3CN. The PEG_6-thiolate-coated $CuInSe_2$ NCs were prepared via ligand exchange reaction of OLA-coated NCs (see Methods Section for detailed procedure).

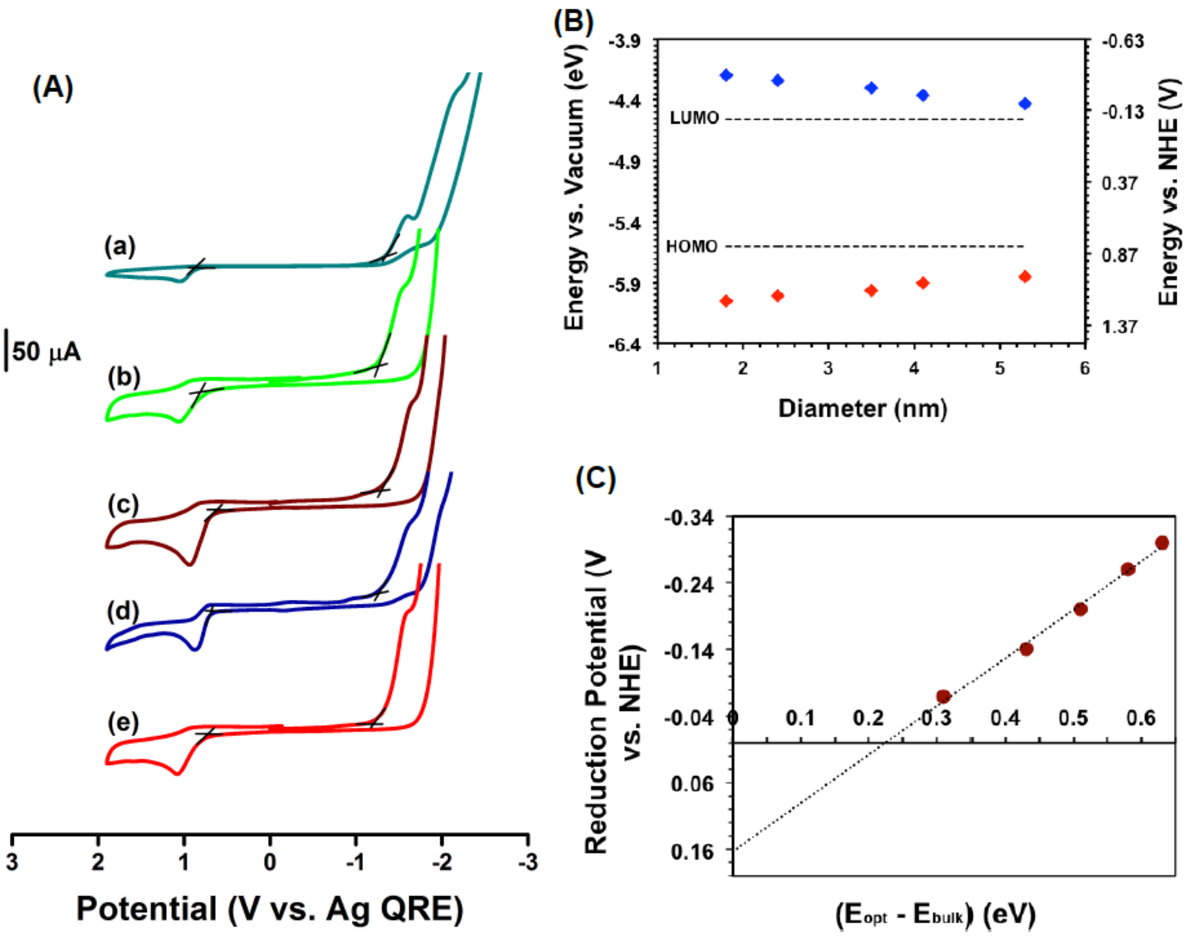

Figure 5. (A) Size dependent CV of PEG$_6$-thiolate-coated $CuInSe_2$ NCs, (a) 1.8, (b) 2.4, (c) 3.5, (d) 4.1, and 5.3 nm in diameter, in a Bu_4NPF_6/CH_3CN solution at a potential scan rate of 0.1 V/s with a 3.0 mm glassy carbon working electrode, Pt wire counter electrode, and Ag wire quasi reference electrode (QRE). (B) The HOMO and LUMO positions of different sizes $CuInSe_2$ NCs determined from CV shown in A. The dotted lines represent HOMO and LUMO position of bulk $CuInSe_2$. (C) The relationship between reduction potential of $CuInSe_2$ NCs and confinement energy, R^2 = 0.993. A direct band-gap of 1.04 eV for bulk $CuInSe_2$ was used for the confinement energy calculation.[25, 26]

^{1}H NMR spectrum showed the disappearance of double bond peak of the OLA at 5.4 ppm, confirming the $CuInSe_2$ NCs were coated with PEG_6-thiolate after the exchange reaction (Figure S6A). Furthermore, as shown in Figure 4A, PEG_6-thiolate-coated NCs were soluble in a diverse range of solvents, indicating the surface of the NCs was coated with PEG_6-thiolate since OLA-coated NCs are not soluble in solvents such as water, ethanol, and acetonitrile. UV-visible spectroscopic (Figure 4B) and TEM (Figure S6B) analyses showed no distinct difference in the optical property and size of $CuInSe_2$ NCs before and after PEG_6-thiolate exchange, suggesting that the NCs maintained their electronic and structural properties.

Figure 5A illustrates the CV of PEG_6-thiolate-coated, different sizes of $CuInSe_2$ NCs in Bu_4NPF_6/CH_3CN electrolyte solution. Clean voltammograms without the presence of additional peaks were observed from which the HOMO and LUMO positions and E_{gap}^{el} were determined (Figure 5B). Even though very clean CVs of gold nanoparticles are reported in the literature,[75, 76] to the best of our knowledge, these are the most pristine voltammograms reported in the literature for ligand-coated semiconductor NCs. As expected, the position of the HOMO shifted to more positive (on NHE scale) and LUMO towards more negative (on NHE scale) with decreasing size, which is in agreement with the theoretical calculations. The position of LUMO could approximately be defined as the reduction potential of the $CuInSe_2$ NC. Therefore, a plot of reduction potential (vs. NHE) versus confinement energy (optical band-gap minus bulk band gap of 1.04 eV) showed a linear relationship as demonstrated in Figure 5C. The bulk reduction potential was calculated from the extrapolation to zero confinement energy and determined to be 0.16 V (vs. NHE). As mentioned for CdSe QDs,[77] this bulk reduction potential should be the *"flat band"* potential of PEG_6-thiolate-coated bulk $CuInSe_2$ in Bu_4NPF_6/CH_3CN solution. Our flat band potential value of $CuInSe_2$ is comparable to the previous report of 0.15 V determined from Mott-Schottky plot.[78]

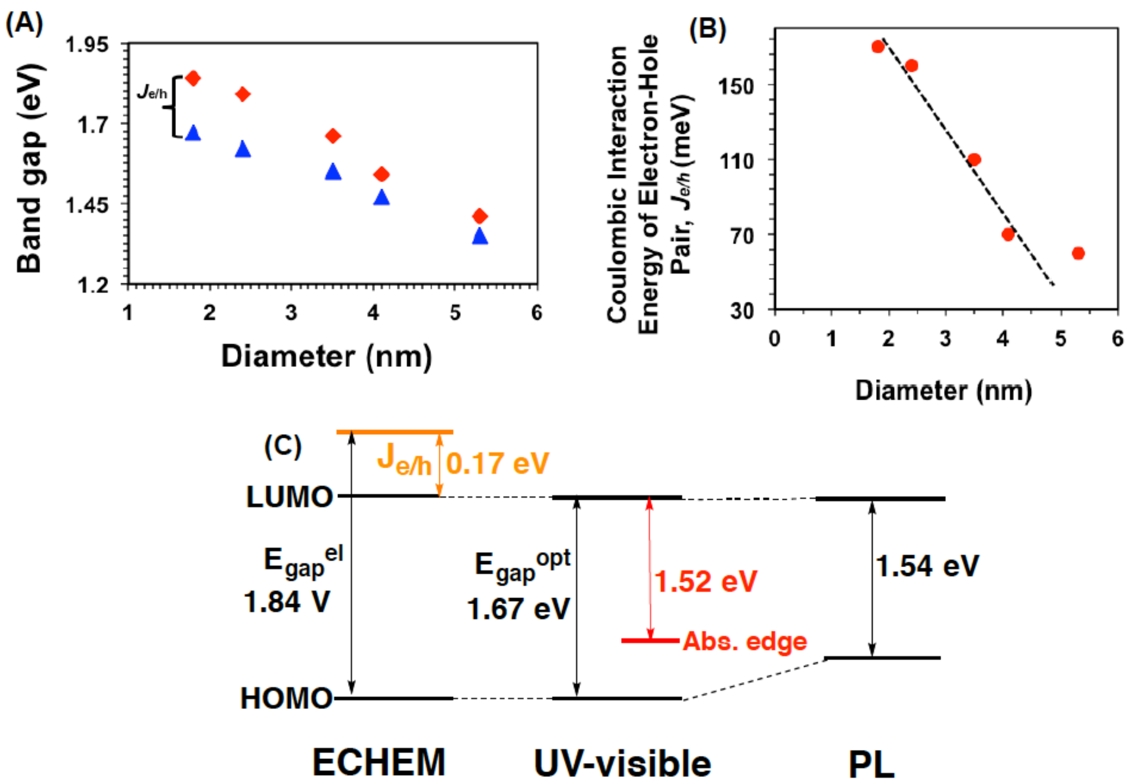

Figure 6. (A) Comparison of size-dependent electrochemical (red diamonds) and optical (blue triangles) band-gaps of PEG_6-thiolate-coated $CuInSe_2$ NCs. (B) Coulombic interaction energy of electron-hole pairs (Je/h) as a function of NC diameter. (C) A schematic diagram representing rough energy level of PEG_6-thiolate-coated 1.8 nm diameter $CuInSe_2$ NCs considering solvent has negligible effects on band-gap and energy level position. The absorption edge was determined from Tauc plot (see Figure S7). The image is not to scale.

As shown in Figure 6A, we observed $E_{gap}^{el} > E_{gap}^{opt}$ and the difference between them could approximately define as $J_{e/h}$, which reduces with decreasing NCs size (Figure 5C).

Interestingly, the $J_{e/h}$ is nearly 90 meV higher for PEG_6-thiolate coating than OLA for 1.8 nm $CuInSe_2$ NCs. This is because the replacement of OLA by PEG_6-thiolate shifts the LUMO towards more positive on the vacuum scale (more negative vs. NHE), thus increasing the E_{gap}^{el}. Such a large difference is not surprising. It is reported that the interaction of electron donating ligands (e.g., thiols) with bulk CdSe electrodes could shift the reduction potential more than 500 mV in the negative direction (vs. NHE).[79] Our result is in agreement with the previous report on electrochemical characterization of trioctylphisphine oxide (TOPO)- and DDT-capped CdSe QDs in which reduction potential was found to be more negative for DDT than TOPO (vs. NHE).[77] Figure 6B illustrates a comparison of $J_{e/h}$ with PEG_6-thiolate-coated, different sizes $CuInSe_2$ NCs. A linear relationship is observed between $J_{e/h}$ and diameter up to 4.1 nm but 5.3 nm diameter $CuInSe_2$ NCs deviate from linearity. This could be due to presence of nonradiative trap states near to the LUMO, where electrons were injected during the potential scanning before the actual reduction potential of the NCs. Nevertheless, we have shown that the electrochemical analysis of semiconductor NCs could be the simple analytical characterization approach for determining E_{gap}^{el} and $J_{e/h}$, and HOMO and LUMO position without confounding the quantum confinement. This demonstrates the importance of surface ligand coating: appropriate ligands enable measurements in electrochemically suitable solvent/electrolyte systems as shown in this present investigation. Thus, electrochemical techniques could obviate the need of expensive spectroscopic techniques commonly used to determine the band gap and HOMO and LUMO position of semiconductor NCs.[80, 81] Finally, similar to thiolate-protected gold nanoparticles,[76] and CdSe[82] and InAs QDs,[83] we also developed a basic energy level diagram (Figure 6C) of PEG_6-thiolate-coated 1.8 nm diameter $CuInSe_2$ NCs from UV-visible and PL spectroscopic, and CV characterizations.

Size-Dependent Photocatalytic Activity of PEG-thiolate-Coated $CuInSe_2$ NCs. Ternary semiconductor NCs/metal oxide heterostructures are commonly used to investigate the NC-induced catalytic transformation of various substrates under heterogeneous reaction conditions. The excellent solubility property of the PEG_6-thiolate-coated $CuInSe_2$ NCs allowed us to study the size dependent photocatalytic activity for degradation of four different pollutants under visible light irradiation (<450 nm) in water, making our catalytic systems fully sustainable. Now we were poised to test the hypothesis that the largest band-gap (smallest size) $CuInSe_2$ NCs will display the highest photocatalytic degradation efficiency (%) under visible light due to their highest interfacial charge transfer efficiency. To test this hypothesis, we studied photodegradation of phenol as a model system because it is not only water soluble but also a commonly found pollutant in petroleum products.

To investigate the size-dependence of photocatalytic activity, first PEG_6-thiolate-coated, 1.8 nm diameter $CuInSe_2$ NCs and phenol were dissolved in water, stirred for 30 min under dark and then illuminated with a 350 W xenon arc lamp (light intensity 34.8 mW/cm^2) fitted with a 450 nm cut-off filter for 2 h. The detailed procedure is provided in Materials and Methods section. The phenol decomposition was determined via UV-visible spectrophotometer monitoring of peak intensity (see Figure S8) at 268 nm at different time points. As shown in Figure 7A, nearly 60 and 30% phenol decomposition were observed for 1.6 and 5.3 nm diameter $CuInSe_2$ NCs, respectively. In Figure 7B, the decomposition efficiency compared with the diameter and E_{gap}^{el} were found to be linear. Thus photocatalytic efficiency is a direct function of the E_{gap}^{el} of $CuInSe_2$ NCs in the range of 1.84 to 1.41 eV. One might expect that the smallest diameter $CuInSe_2$ NCs would absorb less total light than the larger NCs and would therefore display the lowest catalytic activity. However, smaller NCs have a larger surface-to-volume ratio that results in a higher density of surface orbitals (e.g., LUMOs), more similar to isolated molecules when compared to larger NCs. Therefore, interfacial charge transfer is directly related to the size of the NCs, where the smallest NCs are expected to display the highest rate of interfacial electron transfer from NCs to acceptors.[12, 14] Perhaps, interfacial charge transfer (highest for smallest NCs) is a more important factor than light absorption by NCs (highest for largest NCs). It is clear that the size-dependent photocatalytic activity agrees nicely with the literature, where the highest rate of photocatalytic hydrogen evolution was observed for the smallest size CdSe QDs dispersed in an aqueous medium[18] and is also in agreement with theoretical prediction.[83]

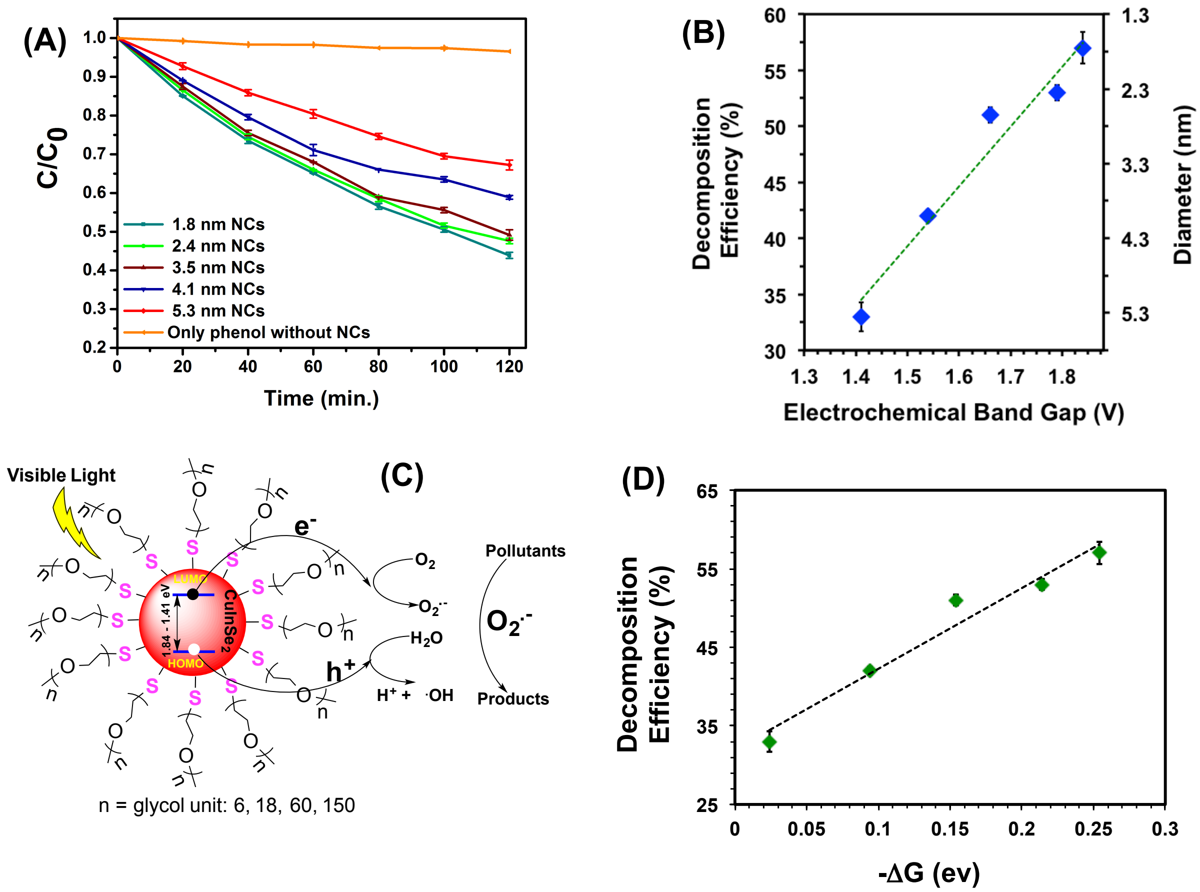

Figure 7. (A) Photo-decomposition efficiency of phenol using PEG_6-thiolate-coated, different sized $CuInSe_2$ NCs under irradiation of visible light (<450 nm). (B) Decomposition efficiency as a function of electrochemical band-gap and diameter, showing linear relationship, R^2 = 0.957. (C) Schematic representation of photoexcitation to generate electrons and holes, followed by reduction of O_2 and oxidation of H_2O, respectively. Photogenerated O_2•− performs photodegradation of pollutants. (D) The dependence of decomposition efficiency on the thermodynamic driving force for the electron transfer, R^2 = 0.961.

We propose that the photocatalytic decomposition of phenol is initiated by the O_2•− as shown in Figure 7C as a second step of the process, and according to our mechanism the first step involves photoexcited electron transfer from $CuInSe_2$ NCs to O_2 followed by one electron reduction of O_2 to O_2•− which is the rate limiting step. In order to investigate the electron transfer mechanism we performed a controlled experiment in which 1.2 x 10^{-5} M benzoquinone (BQ) was added into an aqueous solution containing 5.0 x 10^{-3} M and 1.2 x 10^{-7} M of phenol and PEG_6-thiolate-coated 1.8 $CuInSe_2$ NCs, respectively. After 120 min of light illumination (light intensity, 34.8 mW/cm^2), <8% phenol decomposition was observed (see Figure S9). In contrast, when the same batch of NCs was used to perform the identical photocatalytic reaction without BQ, we determined nearly 56% decomposition efficiency. According to the literature, BQ scavenges the photogenerated electrons before they can react with O_2 to form O_2•−, thereby preventing the photocatalytic reaction,[84, 85] as observed in our investigation. Taken together, the control experiment supports our hypothesis of an electron transfer process that generates O_2•− in order to initiate pollutant decomposition.

The photoexcited electrons undergo thermodynamically-controlled interfacial charge transfer and react with dissolved O_2. We have determined that the first order rate (min^{-1}) of decomposition with respect to E_{gap}^{el} (size) is small (See Figure S10). Moreover, our photocatalytic reaction was performed under homogeneous condition, therefore interfacial (solid-liquid) kinetics - possibly one electron reduction of O_2 to O_2•− - could be the rate-limiting step not the mass transport of the reactants to the $CuInSe_2$ NCs surface.[86] Moreover, oxygen reduction in water is an *inner-sphere* electron transfer reaction.[65] Therefore, we also suggest that the $CuInSe_2$ NC-induced reduction of O_2 to O_2•− follows an inner-sphere electron transfer mechanism, similar to literature report for the metalloenzyme, Cu-amine oxidase.[87] According to Marcus theory, under such circumstances[88, 89] the electron transfer rate constant from donor (e.g., $CuInSe_2$ NCs) to acceptor (e.g., O_2) under homogenous reaction conditions depends on -ΔG and follows Eq. 2.[18, 90]

$$k_{red} \propto exp\left(-\frac{(\Delta G-\lambda)^2}{4kT\lambda}\right) \quad (2)$$

Here, k_{red} is the electron transfer rate constant, and λ and k are the reorganization energy and Boltzmann constant, respectively. The thermodynamic driving force, ΔG, is the electrochemical energy difference between the acceptor and donor systems.[91] In the case of the semiconductor-electrolyte interface, ΔG is the difference between the quasi Fermi level of the semiconductor and acceptor.[16,91] However, in the case of QDs, the Fermi level is generally estimated as the conduction band-edge potential.[2, 12, 90] Based on our electrochemical characterization of $CuInSe_2$ NCs, we determined these energy levels were the HOMO and LUMO levels. Therefore, we could determine the ΔG as the difference between the LUMO of the $CuInSe_2$ NCs and the oxygen reduction potential (E_{red}^0, -0.046 vs. NHE).[92] We calculated the ΔG from Eq. 3 utilizing the LUMO position for PEG_6-thiolate-coated different sizes $CuInSe_2$ NCs as shown in Figure 5B.

$$\Delta G = -e(E_{LUMO} - E_{red}^0) \quad (3)$$

The inner-sphere electron transfer mechanism is very complicated, and will require in-depth analysis under various experimental conditions that are not within the scope of this manuscript. In Figure 7D, the decomposition efficiency compared with the -ΔG is found to be linear where a strong driving force is observed for smallest NCs. We would expect such thermodynamic behavior, because as the size decreases, the LUMO of NCs shifts towards more negative (vs. NHE) making ΔG more negative. Thus, position of the LUMO of $CuInSe_2$ NCs is critical solid-liquid charge transfer, which eventually controls the rate of transformation of O_2 to $O_2{\bullet}-$. The experimental data presented here nicely corroborate with the previous studies demonstrating the size dependent electron transfer process in solid-solid interface (CdSe QD-TiO_2 conjugates), where the smallest size displays the highest transfer rate constant.[12, 14] Finally, we present a qualitative free-energy vs. reaction coordinate diagram for an electron transfer reaction and reduction of O_2 to $O_2{\bullet}-$.[16]

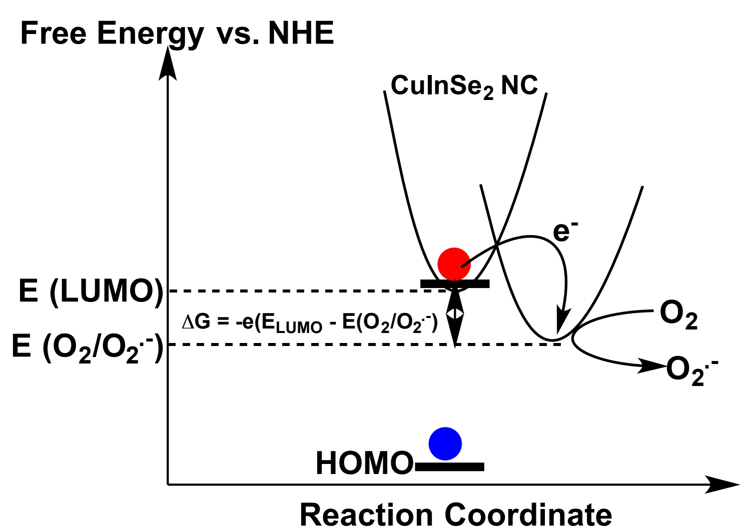

Figure 8. Change in free energy as a function of reaction coordinates for O_2 to $O_2{\bullet}-$ reduction[16] under homogeneous condition in which O_2 reacts at the surface of $CuInSe_2$ NCs. The electron (red dot)-hole (blue dot) pair is generated under illumination of visible light. The thermodynamic driving force for electron transfer can be defined as $\Delta G = -e\left(E_{LUMO} - E^0_{(O_2/\ O_2^{\cdot-})}\right)$. To simplify this energy diagram, the contribution of solvent molecules in activation energy was not considered.

We also compared the decomposition efficiency with the $J_{e/h}$ because one may expect that higher $J_{e/h}$ value (smallest NCs, see Figure 6B) suppresses the charge separation, resulting in slow interfacial charge transfer and low catalytic activity. As shown in Figure S11, a nearly linear relationship between $J_{e/h}$ with respect to decomposition efficiency was observed for diameters $\leq$ 4.1 nm. Moreover, computational studies have shown that the electron-hole recombination probability increases with an increase in $J_{e/h}$ and decrease in NC size[93] that effectively hinders the interfacial charge transfer as well. In this context, perhaps, it is also not surprising that the 1.6 nm diameter $CuInSe_2$ NCs displayed the highest photocatalytic activity. Theoretical calculations have shown that the kinetic energy of electrons and/or holes is higher than the $J_{e/h}$ for smaller sized NCs,[31] which would facilitate the expansion of electron wave functions inside the inorganic core easily, leak through the core boundary, and promote the charge transfer process in the solid-liquid interface.

Taken together, size dependence – a combination of ΔG, $J_{e/h}$, and kinetic energy of the electrons - photocatalytic activity of PEG_6-thiolate-coated $CuInSe_2$ NCs demonstrated above is the first example of its kind, thus obviating the need for large-band gap semiconductors, which act as electron collectors and perform the catalytic reactions.[15, 27, 28] Moreover, the $CuInSe_2$ NCs were stable during the catalytic reaction in water (see Figure S12) without the use of hole scavengers, which makes the reaction conditions sustainable. It is known that in many systems photogenerated holes decompose the semiconductor NCs and to prevent such degradation, sacrificial hole scavengers are commonly used either in liquid junction solar cells[94] or photocatalytic reactions.[2, 16] However, in our system, the excellent solubility property of PEG_6-thiolate-coated $CuInSe_2$ NCs in water appear to allow the photogenerated holes to oxidize water to H^+ and $OH^\bullet$ and prevent the NCs decomposition (Figure 7C). Unlike the long-chain hydrophobic ligand OLA, which inhibits charge transport, PEG_6 chains are capable of transporting photogenerated charges effectively and inducing the formation of O_2•−, resulting in an observed catalytic reaction. Recently, we have shown that PEG_6-thiolate-coated CdSe QDs display unprecedented stability under harsh experimental condition such as light and air[95] that are essential for photocatalytic reaction. Therefore, it is extremely important to investigate the effects of surface passivating ligands chemical structures on photocatalytic activity of $CuInSe_2$ NCs under our experimental conditions, as discussed below.

Effect of Surface Ligand Chemistry on Photocatalytic Properties of $CuInSe_2$ NCs. Semiconductor NC surface ligands not only determine solubility properties, they also control the effective charge transport through ligand monolayers, where insulating ligands (e.g., OLA) impede efficient transport of charge carriers. We hypothesized that the longest PEG_n chains (n = 150) would enable the slowest charge transport through the ligand monolayer and the lowest photocatalytic activity due to the thick insulating barrier around the NCs. To evaluate the role of surface passivating ligands on photocatalytic activity, we utilized 1.8 nm diameter $CuInSe_2$ NCs with different PEG ligands (See Figure 7C), and finally we compared the experimental data with OLA-coated $CuInSe_2$ NCs under identical reaction conditions.

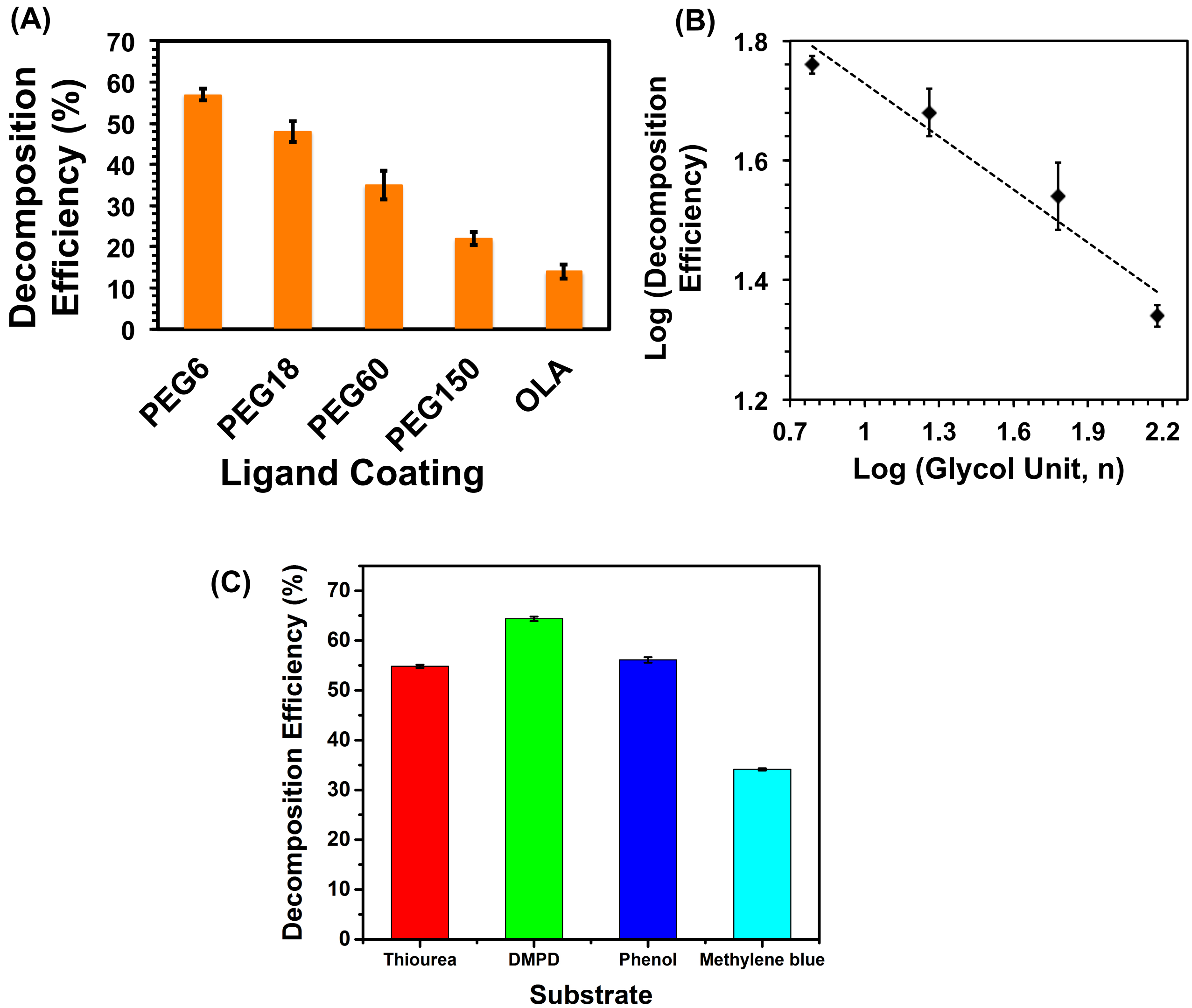

Figure 9. (A) A comparison of photocatalytic phenol decomposition efficiency of 1.8 nm diameter $CuInSe_2$ NCs coated with different chain length PEG_n-thiolate and OLA under illumination of visible light <450 nm for 2h. (B) Log of decomposition efficiency versus log of glycol unit (n), where n = 6, 18, 60, 150. (C) Photocatalytic decomposition efficiency of various water soluble pollutants utilizing PEG_6-thiolate-coated, 1.8 nm diameter $CuInSe_2$ NCs under illumination of visible light (<450 nm) for 2 h.

Photocatalytic decomposition efficiency of $CuInSe_2$ NCs as a function of PEG chain length is shown in Figure 9A and Figure S13. The NCs coated with the shortest PEG_6 chain displayed highest catalytic efficiency. According to calculation (ChemBioDraw 14.0) the fully stretched length of PEG_6- and PEG_{18}-thiolate is ~2.2 and 6.2 nm, respectively. Therefore, a 4.4 nm difference in chain length resulted in ~10% decrease in the degradation efficiency. Importantly, the degradation efficiencies of PEG_6-thiolate-coated NCs were at least four fold higher than the OLA-coated $CuInSe_2$ NCs. interestingly, the photocatalytic activity of even the PEG_{150}-thiolate-coated NCs is nearly comparable to the insulating ligand- (OLA) coated NCs. Therefore, the PEG_{150} layer (too thick for an effective transport of photogenerated charge carriers) behaves as an insulating ligand layer. A log-log plot of decomposition efficiency versus glycol unit (n) shows that the decomposition efficiency follows negative power of n function. The experimental data proved our hypothesis that as PEG_n chain length increases, it behaves like an insulating barrier, which hinders the charge transport and reduce photocatalytic activity. We believe in this case, charge transfer at the solid-liquid interface is not the controlling factor since same the size NCs were used for the catalytic reaction, instead the thickness of the ligand monolayer determines the efficiency, where the shorter and more conductive ligand monolayer is ideal for most the effective photocatalytic reaction. Based on our previous stability studies on PEG_n-thiolate-coated CdSe QDs, we would expect a greater stability for PEG_{150}-thiolate-coated $CuInSe_2$ NCs, which is extremely important for a sustainable photocatalyst, but their slow charge transport properties would effectively hinder their potential use.

Finally, in order to generalize the effectiveness of our photocatalysts, we studied the photocatalytic activity of our PEG_6-thiolate-coated 1.8 nm diameter $CuInSe_2$ NCs for degradation of a diverse range of pollutants, including those that are colorless, see Figure 9C. The semiconductor NC-mediated photocatalytic efficiency is generally studied using dye degradation as a model system. Colorless pollutants do not display photoexcitation like dyes do because of the band gap in the UV region of the solar spectrum, thus it is more difficult to perform their photodegradation under illumination of visible light. Importantly, we demonstrated photodegradation of pollutants such as phenol, N,N-dimethyl-p-phenylenediamine (DMPD), and thiourea, in which PEG_6-thiolate-coated 1.8 nm diameter $CuInSe_2$ NCs acted as the best photocatalyst for decomposition of DMPD (decomposition efficiency = 65%), demonstrating the unique catalytic behavior under our experimental conditions.

Large band-gap metal oxides are often used to extract the photogenerated charges from semiconductor NCs in order to enhance catalysts performances. Here we show that good photocatalytic efficiency of semiconductor NCs could be achieved without the use of metal oxide by simply coating the $CuInSe_2$ NCs surface with short chain, PEG_6-thiolate. Therefore, surface ligand chemistry plays a very significant role not only to enhance the solubility properties for a homogeneous catalytic reaction, but also obviates the need for metal oxide to extract photogenerated charges. We found it surprising that PEG_6-thiolate-coated $CuInSe_2$ NCs were stable during photocatalytic reaction in water and light. We believe that due to covalent character of Cu-S and In-S bonds, $CuInSe_2$ NCs displayed an excellent stability property than literature report demonstrating stability of alkylthiolate-coated QDs (e.g., CdSe QDs) in water under light illumination.[96]

We found that using our PEG_n-thiolate-coated $CuInSe_2$ NCs, the degradation rate constant is significantly low (Figure S8). This could be due to the presence of presence of surface defects that hinder the effective interfacial charge transfer. Therefore, with an appropriate surface coating, the formation of nonradiative trap states could be prevented, resulting in enhanced catalytic performance. Another important aspect would be promoting faster charge separation; attaching surface ligands, which are capable of forming interfacial orbitals with NCs and allow hole wave functions expansion to ligand monolayer[97] that would facilitate the interfacial electron transfer processes. Moreover, stabilizing photogenerated holes will also enhance the long-term stability of the nanomaterials. Taken together, we believe a mixed surface ligation, PEG_n-thiolates and hole accepting ligands, will allow the preparation of unique nanomaterials with unprecedented photocatalytic activity for either hydrogen production[16] or oxygen evolution,[86] which are under our investigation.

CONCLUSION

In conclusion, we have presented, for the first time, the structure-property relationship of ligand-coated $CuInSe_2$ NCs for visible light driven photocatalytic efficiency under homogeneous conditions, where the smallest NCs displayed the highest decomposition efficiency of pollutants in water. The success of this investigation relied heavily on exchanging the native, insulating OLA ligands with more conductive PEG_n-thiolates. The PEG_n-thiolate-coated $CuInSe_2$ NCs have displayed unique solubility properties that have allowed us to perform solution-phase electrochemical analysis, which provided quantitative information about the thermodynamic driving forces for molecular oxygen reduction as a consequence from facile electron transfer at the solid-liquid interface. Our studies have demonstrated that the free energy of electron transfer is the most dominating factor than the capability of visible light absorption and/or probability of electron-hole recombination of NCs. Finally, we have also shown that the appropriate selection of surface ligand's chemical structure is also extremely crucial to the photocatalytic performances of $CuInSe_2$ NCs NCs due to the ability to improve charge transport efficiency through ligand monolayers. We believe, these findings will expedite the quantitative electrochemical characterization of semiconductor NCs in general, and will open up new avenues to design highly efficient, sustainable photocatalysts.

EXPERIMENTAL METHOD

Materials. Copper(I) chloride (CuCl, 99.99%), indium(III)chloride ($InCl_3$, 98%), elemental selenium (pellets, 99.9%), oleylamine (OLA, 70%), 1-hexanethiol (HT) (95%), phenol (99%), thiourea (>99%), N,N-dimethyl-p-phenylenediamine (DMPD, 97%) and methylene blue (MB, 95%), toluene (HPLC grade), ethanol (98.5%), hexanes (99%), chloroform (>99%), dichloromethane (DCM, >99%), ethyl acetate (99.5%), benzoquinone (BQ) and tetrahydrofuran (99.9%) were purchased from Sigma-Aldrich. Sureseal acetonitrile (CH_3CN), DCM, and toluene were also purchased from Sigma-Aldrich. All chemicals were used as received without any further purification. Different chain length polyethylene glycol thiols [PEG_n-SH (n= 6, 18, 60, and 150)] were synthesized according to our published procedure.[72]

Size-Dependent Synthesis of Oleylamine-Coated $CuInSe_2$ NCs. In a N_2-filled glove box, CuCl (0.033 g, 0.33 mmol) $InCl_3$ (0.273 g, 1.23 mmol), and 7.5 mL degassed OLA were loaded into a 25 mL two-neck flask. The flask was sealed, removed from glove box, and attached to a Schlenk line. The reaction mixture was heated at desired growth temperature (see Table 1) under vacuum with stirring for 2 hr and then transferred to N_2 and heated for additional 1 hr. The Se-precursor was separately prepared by dissolving 0.240 g of freshly ground Se powder in a mixture of 3.14 mL OLA and 0.860 mL HT at room temperature and stirred for 90 min. under N_2 atmosphere at room temperature (*Caution: Selenium is toxic, and as such, human exposure should be minimized)*. A 0.8 mL Se-precursor (0.608 mmol) was injected in the metal precursor and the reaction was allowed to proceed for 2 hr. The NCs growth was quenched by injecting 20 mL of toluene. The NCs were purified by drop wise addition of ethanol (~20 mL) and centrifuged at 5000 rpm for 5 min) to yield a brown solid. The solid then redisperssed in toluene (10 mL) and precipitated with ethanol (5 mL). This purification technique was followed once more and then $CuInSe_2$ NCs were dried by blowing N_2 and stored inside the glovebox for further characterization.

Ligand Exchange Reaction with PEGn-thiols (n = 6, 18, 60, 150). Purified OLA-capped $CuInSe_2$ SNCs were dissolved in 5 mL of nitrogen-purged chloroform to obtain a concentration of 1 mM. PEG_6-SH (0.1 mmol) was added to the OLA-coated $CuInSe_2$ SNCs at room temperature and stirred (~12 h) under N_2. To remove excess PEG_6-SH, the solution was then brought to dryness and the solid was redissolved in a minimum amount of chloroform and precipitated with hexane. The resulting solid was collected by centrifugation (7000 rpm, 5 min).

Optical Spectroscopy Characterization. UV−vis absorption spectra were collected using a Varian Cary 50 UV−vis spectrophotometer scanning through a range of 300−1100 nm. All spectra were collected in toluene to determine the optical band gap. Toluene was used as a background for these measurements, and the background was run before collecting the absorbance spectra. The photoluminescence emission (PL) spectra were recorded using a Cary Eclipse fluorescence spectrophotometer from Varian Instruments using 600 nm excitation.

Structural Characterization by TEM, XRD, and ^{1}H NMR. For high-resolution TEM analysis, samples were prepared by placing 10 μL of dissolved $CuInSe_2$ NCs in toluene onto a formver coated copper grid (Electron Microscopy Science). The sample was allowed to sit for 30 sec and any excess solution was removed by wicking with a Kimwipe to avoid particle aggregation. Images were obtained using a JEOL-3200FS-JEM instrument at 200 kV beam energy. The diameter of $CuInSe_2$ NCs was determined using ImageJ software. At least 300 NCs were counted to determine the average size. Wide-angle XRD was recorded on a Rigaku MiniFlex™ II (Cu Kα) instrument. Dry samples (typically ~2-4 mg) were placed in a hole of the sample holder and secured on both sides using Kapton tape. ^{1}H NMR was recorded on a Bruker AVANCE III 500 instrument at 500 MHz. Typically 6 mg of sample were dissolved in 0.6 mL of $CDCl_3$ at room temperature and a minimum of 1000 scans were collected.

Elemental Analysis. A field-emission scanning electron microscopy (FE-SEM) system, which was equipped with a energy dispersive X-ray (EDS) was used to determine the composition of $CuInSe_2$ NCs.

Electrochemical Characterization. Voltammetry was done with a CH Instruments (Austin, TX) model 760D electrochemical analyzer in a conventional three electrodes set-up, which was constructed of a 3.0 mm glassy carbon disk working electrode, a Pt wire counter electrode, and a 0.6 mm diameter Ag wire quasi-reference electrode (QRE). Prior to use, the working electrode was polished with a diamond polishing compound (Buehler), washed with nanopure water, sonicated for 10 min in nanopure water, washed with DCM, and finally dried with N_2. All electrochemical measurements were conducted inside a nitrogen filled glovebox, and sureseal solvents were used for the analysis. A 3.0 ml solution of 0.1 M Bu_4NPF_6, containing 0.02 mmol $CuInSe_2$ NCs was used for CV analysis. The scan rate for all samples was 0.1 V/s. The potential of the Ag QRE was calibrated using Fc/Fc^+ redox couple in acetonitrile vs. Ag/AgCl/3 M KCl (aq) and then converted versus absolute scale (eV) or normal hydrogen electrode (NHE).

Photocatalytic Activity Measurement. The photocatalytic studies were carried out using a 350 W xenon arc lamp (Oriel, Newport Corporation), which was fitted with a 450 nm cut-off filter (light intensity 34.8 mW/cm^2). Irradiation was carried out via side-on illumination onto a 20 mL glass vowel placed 9.0 cm away from the lens adapter. Phenol was chosen as standard substrate to investigate the photocatalytic performance of PEG_n-thiolate-coated $CuInSe_2$ NCs. In a typical experimental set-up, the photocatalyst (1.2 x10^{-7} M) and phenol (5 x 10^{-3} M) were dissolved in water in a 20 mL glass vial with a total volume of 10 mL. The homogeneous solution was stirred for 20 minute under dark with closed capped and then irradiated with light source. To monitor the reaction progress, 70 μl of the reaction mixture was diluted with 3 mL of water and then the concentration of the phenol was determined by measuring the maximum absorbance at 268 nm considering $C/C_0 = A/A_0$. The degradation efficiency and the pseudo-first-order kinetics of the NCs was then determined using Eq. 4 and Eq. 5, respectively:

$$\text{Decomposition efficiency (\%)} = \frac{C_0 - C}{C_0} \times 100 \qquad (4)$$

$$\text{Pseudo-first-order kinetics, } \ln(C/C_0) = -kt \qquad (5)$$

Where C_0 and C are the concentration of phenol before (t = 0) and after (t) light irradiation, respectively, during the photocatalytic reaction. k is the pseudo-first-order rate constant. The same protocol was followed to study the degradation of thiourea, N,N-Dimethyl-p-phenylenediamine, and methylene blue, monitoring the absorption maximum at 235 nm, 242 nm and 664 nm, respectively (Figure S14). We also determined the pseudo-first-order rate constant of phenol degradation using PEG6-thiolate-coated $CuInSe_2$ NCs of different sizes, as shown in Figure S15. For OLA-coated $CuInSe_2$ NCs, prior to measure UV-visible absorbance, the aliquot was centrifuged at 7000 rpm for 2 minute, and then supernatant was diluted with 3 ml water.

ASSOCIATED CONTENT

Supporting Information Available. Additional optical characterization, histograms, TEM image, cyclic voltammograms, graphs, and tables. This material is available free of charge via the Internet at http://pubs.acs.org.

AUTHOR INFORMATION

Corresponding Author

*rsardar@iupui.edu

Author Contributions

#These authors contributed equally to this work.

Notes

Any additional relevant notes should be placed here.

ACKNOWLEDGMENT

The research was partially supported by IUPUI startup funds and IUPUI-RSFG funding. A.J. acknowledges financial support from the Integrated Nanosystems Development Institute (INDI) at IUPUI. We would also like to thank Drs. B. B. Muhoberac and A. J. Siegel for helpful discussion.

REFERENCES

1. Kudo, A.; Miseki, Y. Heterogeneous photocatalyst materials for water splitting. *Chem. Soc. Rev.* **2009**, *38*, 253-278.
2. Osterloh, F. E. Inorganic nanostructures for photoelectrochemical and photocatalytic water splitting. *Chem. Soc. Rev.* **2013**, *42*, 2294-2320.
3. Maeda, K.; Domen, K. Photocatalytic Water Splitting: Recent Progress and Future Challenges. *J. Phys. Chem. Lett.* **2010**, *1*, 2655-2661.
4. Serpone, N.; Emeline, A. V. Semiconductor Photocatalysis-Past, Present, and Future Outlook. *J. Phys. Chem. Lett.* **2012**, *3*, 673-677.
5. Fan, W.; Zhang, Q.; Wang, Y. Semiconductor-based nanocomposites for photocatalytic H2 production and CO2 conversion. *Phys. Chem. Chem. Phys.* **2013**, *15*, 2632-2649.
6. Lewis, N. S.; Nocera, D. G. Powering the planet: Chemical challenges in solar energy utilization. *Proc. Natl. Acad. Sci.* **2006**, *103*, 15729-15735.
7. Harris, C.; Kamat, P. V. Photocatalysis with CdSe Nanoparticles in Confined Media: Mapping Charge Transfer Events in the Subpicosecond to Second Timescales. *ACS Nano* **2009**, *3*, 682-690.
8. Peterson, M. D.; Cass, L. C.; Harris, R. D.; Edme, K.; Sung, K.; Weiss, E. A. The Role of Ligands in Determining the Exciton Relaxation Dynamics in Semiconductor Quantum Dots. *Ann. Rev. Mater. Sci.* **2014**, *65*, 317-339.
9. Scholes, G. D.; Jones, M.; Kumar, S. Energetics of Photoinduced Electron-Transfer Reactions Decided by Quantum Confinement. *J. Phys. Chem. C* **2007**, *111*, 13777-13785.
10. Xie, Y.; Teunis, M. B.; Pandit, B.; Sardar, R.; Liu, J. Molecule-like CdSe Nanoclusters Passivated with Strongly Interacting Ligands: Energy Level Alignment and Photoinduced Ultrafast Charge Transfer Processes. *J. Phys. Chem. C* **2015**, *119*, 2813-2821.
11. Kamat, P. V. Manipulation of Charge Transfer Across Semiconductor Interface. A Criterion That Cannot Be Ignored in Photocatalyst Design. *J. Phys. Chem. Lett.* **2012**, *3*, 663-672.
12. Robel, I.; Kuno, M.; Kamat, P. V. Size-Dependent Electron Injection from Excited CdSe Quantum Dots into TiO2 Nanoparticles. *J. Am. Chem. Soc.* **2007**, *129*, 4136-4137.
13. Wu, N.; Wang, J.; Tafen, D. N.; Wang, H.; Zheng, J.-G.; Lewis, J. P.; Liu, X.; Leonard, S. S.; Manivannan, A. Shape-Enhanced Photocatalytic Activity of Single-Crystalline Anatase TiO2 (101) Nanobelts. *J. Am. Chem. Soc.* **2010**, *132*, 6679-6685.
14. Tvrdy, K.; Frantsuzov, P. A.; Kamat, P. V. Photoinduced electron transfer from semiconductor quantum dots to metal oxide nanoparticles. *Proc. Natl. Acad. Sci.* **2011**, *108*, 29-34.
15. Ma, Y.; Wang, X.; Jia, Y.; Chen, X.; Han, H.; Li, C. Titanium Dioxide-Based Nanomaterials for Photocatalytic Fuel Generations. *Chem. Rev.* **2014**, *114*, 9987-10043.
16. Zhao, J.; Holmes, M. A.; Osterloh, F. E. Quantum Confinement Controls Photocatalysis: A Free Energy Analysis for Photocatalytic Proton Reduction at CdSe Nanocrystals. *ACS Nano* **2013**, *7*, 4316-4325.
17. Thibert, A.; Frame, F. A.; Busby, E.; Holmes, M. A.; Osterloh, F. E.; Larsen, D. S. Sequestering High-Energy Electrons to Facilitate Photocatalytic Hydrogen Generation in CdSe/CdS Nanocrystals. *J. Phys. Chem. Lett.* **2011**, *2*, 2688-2694.

18. Holmes, M. A.; Townsend, T. K.; Osterloh, F. E. Quantum confinement controlled photocatalytic water splitting by suspended CdSe nanocrystals. *Chem. Comm.* **2012**, *48*, 371-373.
19. Liang, Y. N.; Yu, K.; Yan, Q.; Hu, X. Colloidal CuInSe2 Nanocrystals: From Gradient Stoichiometry toward Homogeneous Alloyed Structure Mediated by Conducting Polymer P3HT. *ACS Appl. Mater. Interfaces* **2013**, *5*, 4100-4106.
20. Jara, D. H.; Yoon, S. J.; Stamplecoskie, K. G.; Kamat, P. V. Size-Dependent Photovoltaic Performance of CuInS2 Quantum Dot-Sensitized Solar Cells. *Chem. Mater.* **2014**, *26*, 7221-7228.
21. Panthani, M. G.; Stolle, C. J.; Reid, D. K.; Rhee, D. J.; Harvey, T. B.; Akhavan, V. A.; Yu, Y.; Korgel, B. A. CuInSe2 Quantum Dot Solar Cells with High Open-Circuit Voltage. *J. Phys. Chem. Lett.* **2013**, *4*, 2030-2034.
22. Pan, Z.; Mora-Seró, I.; Shen, Q.; Zhang, H.; Li, Y.; Zhao, K.; Wang, J.; Zhong, X.; Bisquert, J. High-Efficiency "Green" Quantum Dot Solar Cells. *J. Am. Chem. Soc.* **2014**, *136*, 9203-9210.
23. Guo, Q.; Kim, S. J.; Kar, M.; Shafarman, W. N.; Birkmire, R. W.; Stach, E. A.; Agrawal, R.; Hillhouse, H. W. Development of CuInSe2 Nanocrystal and Nanoring Inks for Low-Cost Solar Cells. *Nano. Lett.* **2008**, *8*, 2982-2987.
24. Guillemoles, J.-F.; Rau, U.; Kronik, L.; Schock, H.-W.; Cahen, D. Cu(In,Ga)Se2 Solar Cells: Device Stability Based on Chemical Flexibility. *Adv. Mater* **1999**, *11*, 957-961.
25. Rockett, A.; Birkmire, R. W. CuInSe2 for photovoltaic applications. *J. Appl. Phys.* **1991**, *70*, R81-R97.
26. Aldakov, D.; Lefrancois, A.; Reiss, P. Ternary and quaternary metal chalcogenide nanocrystals: synthesis, properties and applications. *J. Mater. Chem. C* **2013**, *1*, 3756-3776.
27. Shen, F.; Que, W.; He, Y.; Yuan, Y.; Yin, X.; Wang, G. Enhanced Photocatalytic Activity of ZnO Microspheres via Hybridization with CuInSe2 and CuInS2 Nanocrystals. *ACS Appl. Mater. Interfaces* **2012**, *4*, 4087-4092.
28. Shen, F.; Que, W.; Liao, Y.; Yin, X. Photocatalytic Activity of TiO2 Nanoparticles Sensitized by CuInS2 Quantum Dots. *Ind. Eng. Chem.* **2011**, *50*, 9131-9137.
29. Kar, M.; Agrawal, R.; Hillhouse, H. W. Formation Pathway of CuInSe2 Nanocrystals for Solar Cells. *J. Am. Chem. Soc.* **2011**, *133*, 17239-17247.
30. Steigerwald, M. L.; Brus, L. E. Semiconductor crystallites: a class of large molecules. *Acc. Chem. Res.* **1990**, *23*, 183–188.
31. Brus, L. E. Electron--electron and electron-hole interactions in small semiconductor crystallites: The size dependence of the lowest excited electronic state. *J. Appl. Phys.* **1984**, *80*, 4403-4409.
32. Yarema, O.; Bozyigit, D.; Rousseau, I.; Nowack, L.; Yarema, M.; Heiss, W.; Wood, V. Highly Luminescent, Size- and Shape-Tunable Copper Indium Selenide Based Colloidal Nanocrystals. *Chem. Mater.* **2013**, *25*, 3753-3757.
33. Reifsnyder, D. C.; Ye, X.; Gordon, T. R.; Song, C.; Murray, C. B. Three-Dimensional Self-Assembly of Chalcopyrite Copper Indium Diselenide Nanocrystals into Oriented Films. *ACS Nano* **2013**, *7*, 4307-4315.
34. Jasieniak, J.; Mulvaney, P. From Cd-Rich to Se-Rich-the Manipulation of CdSe Nanocrystal Surface Stoichiometry. *J. Am. Chem. Soc.* **2007**, *129*, 2841-2848.

35. Anderson, N. C.; Hendricks, M. P.; Choi, J. J.; Owen, J. S. Ligand Exchange and the Stoichiometry of Metal Chalcogenide Nanocrystals: Spectroscopic Observation of Facile Metal-Carboxylate Displacement and Binding. *J. Am. Chem. Soc.* **2013**, *135*, 18536-18548.
36. Knowles, K. E.; Tice, D. B.; McArthur, E. A.; Solomon, G. C.; Weiss, E. A. Chemical Control of the Photoluminescence of CdSe Quantum Dot-Organic Complexes with a Series of Para-Substituted Aniline Ligands. *J. Am. Chem. Soc.* **2009**, *132*, 1041-1050.
37. Moreels, I.; Fritzinger, B.; Martins, J. C.; Hens, Z. Surface Chemistry of Colloidal PbSe Nanocrystals. *J. Am. Chem. Soc.* **2008**, *130*, 15081-15086.
38. Dolai, S.; Nimmala, P. R.; Mandal, M.; Muhoberac, B. B.; Dria, K.; Dass, A.; Sardar, R. Isolation of Bright Blue Light-Emitting CdSe Nanocrystals with 6.5 kDa Core in Gram Scale: High Photoluminescence Efficiency Controlled by Surface Ligand Chemistry. *Chem. Mater.* **2014**, *26*, 1278-1285.
39. Rosson, T. E.; Claiborne, S. M.; McBride, J. R.; Stratton, B. S.; Rosenthal, S. J. Bright White Light Emission from Ultrasmall Cadmium Selenide Nanocrystals. *J. Am. Chem. Soc.* **2012**, *134*, 8006-8009.
40. Cassette, E.; Pons, T.; Bouet, C.; Helle, M.; Bezdetnaya, L.; Marchal, F.; Dubertret, B. Synthesis and Characterization of Near-Infrared Cu–In–Se/ZnS Core/Shell Quantum Dots for In vivo Imaging. *Chem. Mater.* **2010**, *22*, 6117-6124.
41. Tang, J.; Hinds, S.; Kelley, S. O.; Sargent, E. H. Synthesis of Colloidal CuGaSe2, CuInSe2, and Cu(InGa)Se2 Nanoparticles. *Chem. Mater.* **2008**, *20*, 6906-6910.
42. Jiang, C.; Lee, J.-S.; Talapin, D. V. Soluble Precursors for CuInSe2, CuIn1–xGaxSe2, and Cu2ZnSn(S,Se)4 Based on Colloidal Nanocrystals and Molecular Metal Chalcogenide Surface Ligands. *J. Am. Chem. Soc.* **2012**, *134*, 5010-5013.
43. Wang, J.-J.; Wang, Y.-Q.; Cao, F.-F.; Guo, Y.-G.; Wan, L.-J. Synthesis of Monodispersed Wurtzite Structure CuInSe2 Nanocrystals and Their Application in High-Performance Organic–Inorganic Hybrid Photodetectors. *J. Am. Chem. Soc.* **2010**, *132*, 12218-12221.
44. Norako, M. E.; Brutchey, R. L. Synthesis of Metastable Wurtzite CuInSe2 Nanocrystals. *Chem. Mater.* **2010**, *22*, 1613-1615.
45. Xu, J.; Lee, C.-S.; Tang, Y.-B.; Chen, X.; Chen, Z.-H.; Zhang, W.-J.; Lee, S.-T.; Zhang, W.; Yang, Z. Large-Scale Synthesis and Phase Transformation of CuSe, CuInSe2, and CuInSe2/CuInS2 Core/Shell Nanowire Bundles. *ACS Nano* **2010**, *4*, 1845-1850.
46. Koo, B.; Patel, R. N.; Korgel, B. A. Synthesis of CuInSe2 Nanocrystals with Trigonal Pyramidal Shape. *J. Am. Chem. Soc.* **2009**, *131*, 3134-3135.
47. Nose, K.; Omata, T.; Otsuka-Yao-Matsuo, S. Colloidal Synthesis of Ternary Copper Indium Diselenide Quantum Dots and Their Optical Properties. *J. Phys. Chem. C* **2009**, *113*, 3455-3460.
48. Zhong, H.; Wang, Z.; Bovero, E.; Lu, Z.; van Veggel, F. C. J. M.; Scholes, G. D. Colloidal CuInSe2 Nanocrystals in the Quantum Confinement Regime: Synthesis, Optical Properties, and Electroluminescence. *J. Phys. Chem. C* **2011**, *115*, 12396-12402.
49. Allen, P. M.; Bawendi, M. G. Ternary I–III–VI Quantum Dots Luminescent in the Red to Near-Infrared. *J. Am. Chem. Soc.* **2008**, *130*, 9240-9241.
50. Liu, Y.; Yao, D.; Shen, L.; Zhang, H.; Zhang, X.; Yang, B. Alkylthiol-Enabled Se Powder Dissolution in Oleylamine at Room Temperature for the Phosphine-Free

Synthesis of Copper-Based Quaternary Selenide Nanocrystals. *J. Am. Chem. Soc.* **2012**, *134*, 7207-7210.
51. Wang, X.; Liu, X.; Yin, D.; Ke, Y.; Swihart, M. T. Size-, Shape-, and Composition-Controlled Synthesis and Localized Surface Plasmon Resonance of Copper Tin Selenide Nanocrystals. *Chem. Mater.* **2015**, *27*, 3378-3388.
52. Halpert, J. E.; Morgenstern, F. S. F.; Ehrler, B.; Vaynzof, Y.; Credgington, D.; Greenham, N. C. Charge Dynamics in Solution-Processed Nanocrystalline CuInS2 Solar Cells. *ACS Nano* **2015**, *9*, 5857-5867.
53. Amelia, M.; Lincheneau, C.; Silvi, S.; Credi, A. Electrochemical properties of CdSe and CdTe quantum dots. *Chem. Soc. Rev.* **2012**, *41*, 5728-5743.
54. Amelia, M.; Impellizzeri, S.; Monaco, S.; Yildiz, I.; Silvi, S.; Raymo, F. M.; Credi, A. Structural and Size Effects on the Spectroscopic and Redox Properties of CdSe Nanocrystals in Solution: The Role of Defect States. *Chem. Phys. Chem.* **2011**, *12*, 2280-2288.
55. Inamdar, S. N.; Ingole, P. P.; Haram, S. K. Determination of Band Structure Parameters and the Quasi-Particle Gap of CdSe Quantum Dots by Cyclic Voltammetry. *Chem. Phys. Chem.* **2008**, *9*, 2574-2579.
56. Kuçur, E.; Bücking, W.; Arenz, S.; Giernoth, R.; Nann, T. Heterogeneous Charge Transfer of Colloidal Nanocrystals in Ionic Liquids. *Chem. Phys. Chem.* **2006**, *7*, 77-81.
57. Kucur, E.; Riegler, J.; Urban, G. A.; Nann, T. Determination of quantum confinement in CdSe nanocrystals by cyclic voltammetry. *J. Appl. Phys.* **2003**, *119*, 2333-2337.
58. Kucur, E.; Bucking, W.; Giernoth, R.; Nann, T. Determination of Defect States in Semiconductor Nanocrystals by Cyclic Voltammetry. *J. Phys. Chem. C* **2005**, *109*, 20355-20360.
59. Haram, S. K.; Quinn, B. M.; Bard, A. J. Electrochemistry of CdS nanoparticles: a correlation between optical and electrochemical band gaps. *J. Am. Chem. Soc.* **2001**, *123*, 8860-8861.
60. Querner, C.; Reiss, P.; Sadki, S.; Zagorska, M.; Pron, A. Size and ligand effects on the electrochemical and spectroelectrochemical responses of CdSe nanocrystals. *Phys. Chem. Chem. Phys.* **2005**, *7*, 3204-3209.
61. Poznyak, S. K.; Osipovich, N. P.; Shavel, A.; Talapin, D. V.; Gao, M.; Eychmuller, A.; Gaponik, N. Size-dependent electrochemical behavior of thiol-capped CdTe nanocrystals in aqueous solution. *J. Phys. Chem. B* **2005**, *109*, 1094-1100.
62. Bae, Y.; Myung, N.; Bard, A. J. Electrochemistry and Electrogenerated Chemiluminescence of CdTe Nanoparticles. *Nano. Lett.* **2004**, *4*, 1153–1161.
63. Ingole, P. P.; Markad, G. B.; Saraf, D.; Tatikondewar, L.; Nene, O.; Kshirsagar, A.; Haram, S. K. Band Gap Bowing at Nanoscale: Investigation of CdSxSe1−x Alloy Quantum Dots through Cyclic Voltammetry and Density Functional Theory. *J. Phys. Chem. C* **2013**, *117*, 7376-7383.
64. Liu, J.; Yang, W.; Li, Y.; Fan, L.; Li, Y. Electrochemical studies of the effects of the size, ligand and composition on the band structures of CdSe, CdTe and their alloy nanocrystals. *Phys. Chem. Chem. Phys.* **2014**, *16*, 4778-4788.
65. Bard, A. J.; Faulkner, L. R. (2001) *Electrochemical Methods: Fundamentals and Applications* (John Wiley & Sons, Inc) 2nd Ed.
66. Franceschetti, A.; Zunger, A. Pseudopotential calculations of electron and hole addition spectra of InAs, InP, and Si quantum dots. *Phys. Rev. B* **2000**, *62*, 2614-2623.

67. Lesnyak, V.; George, C.; Genovese, A.; Prato, M.; Casu, A.; Ayyappan, S.; Scarpellini, A.; Manna, L. Alloyed Copper Chalcogenide Nanoplatelets via Partial Cation Exchange Reactions. *ACS Nano* **2014**, *8*, 8407-8418.
68. Zhong, H.; Lo, S. S.; Mirkovic, T.; Li, Y.; Ding, Y.; Li, Y.; Scholes, G. D. Noninjection Gram-Scale Synthesis of Monodisperse Pyramidal CuInS2 Nanocrystals and Their Size-Dependent Properties. *ACS Nano* **2010**, *4*, 5253-5262.
69. Ahmadi, M.; Pramana, S. S.; Batabyal, S. K.; Boothroyd, C.; Mhaisalkar, S. G.; Lam, Y. M. Synthesis of Cu2SnSe3 Nanocrystals for Solution Processable Photovoltaic Cells. *Org. Chem.* **2013**, *52*, 1722-1728.
70. Norako, M. E.; Greaney, M. J.; Brutchey, R. L. Synthesis and Characterization of Wurtzite-Phase Copper Tin Selenide Nanocrystals. *J. Am. Chem. Soc.* **2012**, *134*, 23-26.
71. Pradhan, N.; Reifsnyder, D.; Xie, R.; Aldana, J.; Peng, X. Surface Ligand Dynamics in Growth of Nanocrystals. *J. Am. Chem. Soc.* **2007**, *129*, 9500-9509.
72. Lawrence, K. N.; Johnson, M. A.; Dolai, S.; Kumbhar, A.; Sardar, R. Solvent-like ligand-coated ultrasmall cadmium selenide nanocrystals: strong electronic coupling in a self-organized assembly. *Nanoscale* **2015**, *7*, 11667-11677.
73. Williams, M. E.; Murray, R. W. Perylene Polyether Hybrids: Highly Soluble, Luminescent, Redox-Active Dyes. *Chem. Mater.* **1998**, *10*, 3603-3610.
74. Williams, M. E.; Masui, H.; Long, J. W.; Malik, J.; Murray, R. W. Electron and Mass Transport in Hybrid Redox Polyether Melts: Co and Fe Bipyridines with Attached Polyether Chains. *J. Am. Chem. Soc.* **1997**, *119*, 1997-2005.
75. Qian, H.; Zhu, Y.; Jin, R. Size-Focusing Synthesis, Optical and Electrochemical Properties of Monodisperse Au38(SC2H4Ph)24 Nanoclusters. *ACS Nano* **2009**, *3*, 3795-3803.
76. Lee, D.; Donkers, R. L.; Wang, G.; Harper, A. S.; Murray, R. W. Electrochemistry and Optical Absorbance and Luminescence of Molecule-like Au38 Nanoparticles. *J. Am. Chem. Soc.* **2004**, *126*, 6193-6199.
77. Wang, C.; Shim, M.; Guyot-Sionnest, P. Electrochromic Nanocrystal Quantum Dots. *Science* **2001**, *291*, 2390-2392.
78. Ye, H.; Park, H. S.; Akhavan, V. A.; Goodfellow, B. W.; Panthani, M. G.; Korgel, B. A.; Bard, A. J. Photoelectrochemical Characterization of CuInSe2 and Cu(In1−xGax)Se2 Thin Films for Solar Cells. *J. Phys. Chem. C* **2011**, *115*, 234-240.
79. Thackeray, J. W.; Natan, M. J.; Ng, P.; Wrighton, M. S. Interaction of diethyldithiocarbamate with n-type cadmium sulfide and cadmium selenide: efficient photoelectrochemical oxidation to the disulfide and flat-band potential of the semiconductor as a function of adsorbate concentration. *J. Am. Chem. Soc.* **1986**, *108*, 3570-3577.
80. Jasieniak, J.; Califano, M.; Watkins, S. E. Size-Dependent Valence and Conduction Band-Edge Energies of Semiconductor Nanocrystals. *ACS Nano* **2011**, *5*, 5888-5902.
81. Meulenberg, R. W.; Lee, J. R. I.; Wolcott, A.; Zhang, J. Z.; Terminello, L. J.; van Buuren, T. Determination of the Exciton Binding Energy in CdSe Quantum Dots. *ACS Nano* **2009**, *3*, 325-330.
82. Dolai, S.; Dass, A.; Sardar, R. Photophysical and Redox Properties of Molecule-like CdSe Nanoclusters. *Langmuir* **2013**, *29*, 6187-6193.

83. Soreni-Harari, M.; Yaacobi-Gross, N.; Steiner, D.; Aharoni, A.; Banin, U.; Millo, O.; Tessler, N. Tuning Energetic Levels in Nanocrystal Quantum Dots through Surface Manipulations. *Nano. Lett.* **2008**, *8*, 678-684.
84. Bhunia, S. K.; Jana, N. R. Reduced Graphene Oxide-Silver Nanoparticle Composite as Visible Light Photocatalyst for Degradation of Colorless Endocrine Disruptors. *ACS Appl. Mater. Interfaces* **2014**, *6*, 20085-20092.
85. Su, Y.; Peng, L.; Guo, J.; Huang, S.; Lv, L.; Wang, X. Tunable Optical and Photocatalytic Performance Promoted by Nonstoichiometric Control and Site-Selective Codoping of Trivalent Ions in NaTaO3. *The Journal of Physical Chemistry C* **2014**, *118*, 10728-10739.
86. Chen, D. P.; Bowers, W.; Skrabalak, S. E. Aerosol-Assisted Combustion Synthesis of Single-Crystalline NaSbO3 Nanoplates: A Topotactic Template for Ilmenite AgSbO3. *Chem. Mater.* **2015**, *27*, 174-180.
87. Mukherjee, A.; Smirnov, V. V.; Lanci, M. P.; Brown, D. E.; Shepard, E. M.; Dooley, D. M.; Roth, J. P. Inner-Sphere Mechanism for Molecular Oxygen Reduction Catalyzed by Copper Amine Oxidases. *J. Am. Chem. Soc.* **2008**, *130*, 9459-9473.
88. Marcus, R. A. On the Theory of Oxidation-Reduction Reactions Involving Electron Transfer. 1. *J. Chem. Phys.* **1956**, *24*, 966-978.
89. Marcus, R. A. On the Theory of Electron‐Transfer Reactions. VI. Unified Treatment for Homogeneous and Electrode Reactions. *J. Chem. Phys.* **1965**, *43*, 679-701.
90. Gerischer, H. The impact of semiconductors on the concepts of electrochemistry. *Electrochim. Acta* **1990**, *35*, 1677-1699.
91. Memming, R. (1994) Photoinduced charge transfer processes at semiconductor electrodes and particles. *Electron Transfer I,* Topics in Current Chemistry, ed Mattay J (Springer Berlin Heidelberg), Vol 169, pp 105-181.
92. Soltani, N.; Saion, E.; Hussein, M. Z.; Erfani, M.; Abedini, A.; Bahmanrokh, G.; Navasery, M.; Vaziri, P. Visible Light-Induced Degradation of Methylene Blue in the Presence of Photocatalytic ZnS and CdS Nanoparticles. *Int. J. Mol. Sci.* **2012**, *13*, 12242.
93. Elward, J. M.; Chakraborty, A. Effect of Dot Size on Exciton Binding Energy and Electron–Hole Recombination Probability in CdSe Quantum Dots. *J. Chem. Theory Comput.* **2013**, *9*, 4351-4359.
94. Chakrapani, V.; Baker, D.; Kamat, P. V. Understanding the role of the sulfide redox couple (S2-/S(n)2-) in quantum dot-sensitized solar cells. *J. Am. Chem. Soc.* **2011**, *133*, 9607-9615.
95. Lawrence, K.; Dolai, S.; Lin, Y.-H.; Dass, A.; Sardar, R. Enhancing the Physicochemical and Photophysical Properties of Small (<2.0 nm) CdSe Nanoclusters for Intracellular Imaging Applications. *RSC. Adv* **2014**, *4*, 30742-30753.
96. Billone, P. S.; Maretti, L.; Maurel, V.; Scaiano, J. C. Dynamics of the Dissociation of a Disulfide Biradical on a CdSe Nanoparticle Surface. *J. Am. Chem. Soc.* **2007**, *129*, 14150-14151.
97. Frederick, M. T.; Amin, V. A.; Swenson, N. K.; Ho, A. Y.; Weiss, E. A. Control of Exciton Confinement in Quantum Dot-Organic Complexes through Energetic Alignment of Interfacial Orbitals. *Nano. Lett.* **2013**, *13*, 287-292.

TOC Graphic

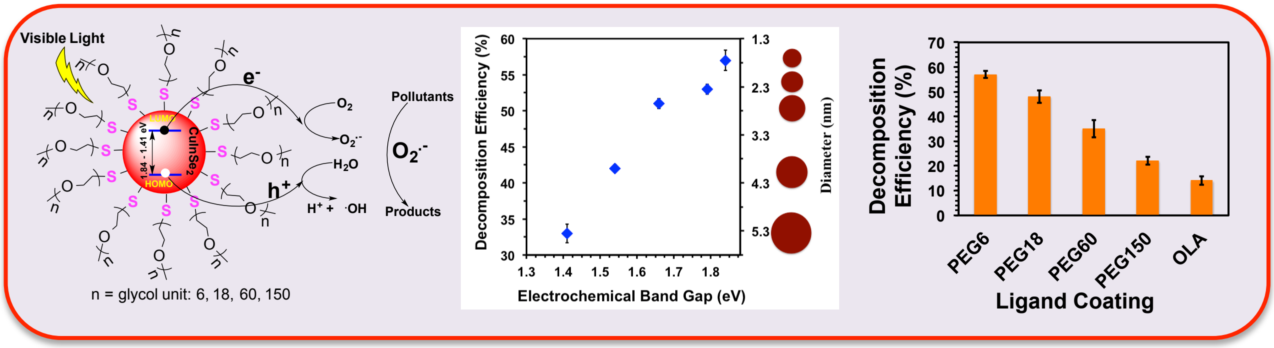

Visible Light
CuInSe2
LUMO
HOMO
1.84 - 1.41 eV
e-
h+
O2
O2·-
H2O
H+ + ·OH
Pollutants
Products
n = glycol unit: 6, 18, 60, 150
Decomposition Efficiency (%)
Electrochemical Band Gap (eV)
Diameter (nm)
Ligand Coating
PEG6
PEG18
PEG60
PEG150
OLA